Hydrothermal origin of elevated iron, manganese and redox-sensitive trace elements in the *c*. 635 Ma Doushantuo cap carbonate

Jing Huang, Xuelei Chu, Ganqing Jiang, et al.

Journal of the Geological Society 2011; v. 168; p. 805-816
doi: 10.1144/0016-76492010-132

Journal of the Geological Society, London, Vol. **168**, 2011, pp. 805–815. doi: 10.1144/0016-76492010-132.

Hydrothermal origin of elevated iron, manganese and redox-sensitive trace elements in the *c*. 635 Ma Doushantuo cap carbonate

JING HUANG[1,2], XUELEI CHU[1,2]*, GANQING JIANG[3], LIANJUN FENG[1] & HUAJIN CHANG[4]

[1]*Institute of Geology and Geophysics, Chinese Academy of Sciences, Beijing 100029, China*

[2]*State Key Laboratory of Lithospheric Evolution, Beijing 100029, China*

[3]*Department of Geoscience, University of Nevada, Las Vegas, NV 89154-4010, USA*

[4]*School of Life and Geography Sciences, Qinghai Normal University, Key Laboratory of Tibetan Plateau Environment and Resources, Ministry of Education, Xining 810008, China*

**Corresponding author (e-mail: xlchu@mail.iggcas.ac.cn)*

Abstract: Major and trace element, including REE, concentrations of the Doushantuo cap carbonate (*c*. 635 Ma) in South China show enrichment in Fe, Mn and redox-sensitive elements and slightly negative Ce anomalies, indicating anoxic environments during cap carbonate precipitation. High Fe_T/Al ratios but very low concentration of extractable pyrites suggest ferruginous rather than euxinic conditions. The REE + Y patterns of samples show enrichment of heavy REE (HREE), positive Eu anomalies and positive Y anomalies, implying a hydrothermal origin for elevated concentration of Fe, Mn and redox-sensitive elements. The results suggest that ferruginous Ediacaran oceans may have rooted from hydrothermally induced iron accumulation in severely glaciated Cryogenian oceans.

Cap carbonates directly overlying Cryogenian glacial diamictites are the critical stratigraphic record for understanding the transition from the Earth's extreme cold to Ediacaran environments that hosted early multicellular organisms. In the last decade, enormous efforts have been made to understand the sedimentological, stratigraphic and isotope geochemical details of cap carbonates, particularly the *c*. 635 Ma cap carbonates overlying the late Cryogenian glaciogenic successions (Kirschvink 1992; Kennedy 1996; Kaufman *et al.* 1997; James *et al.* 2001; Kennedy *et al.* 2001; Hoffman & Schrag 2002; Jiang *et al.* 2003*a*, 2006*a*; Nogueira *et al.* 2003; de Alvarenga *et al.* 2004; Hoffmann *et al.* 2004; Xiao *et al.* 2004; Shen *et al.* 2005; Shields 2005; Hoffman *et al.* 2007; Giddings & Wallace 2009). Although the origin of cap carbonates and associated sedimentary features remains debated (Hoffman & Schrag 2002; Shields 2005; Jiang *et al.* 2006*b*; Fairchild & Kennedy 2007), isotope studies imply that cap carbonates were probably formed in stratified oceanic environments with oxic surface meltwater overlying anoxic deep ocean (Shen *et al.* 2005, 2008; Shields 2005; Hurtgen *et al.* 2006).

A particular phenomenon that has been recently noted but not adequately studied is the high concentration of iron (Fe), manganese (Mn) and other redox-sensitive elements in cap carbonates (Font *et al.* 2006; Nédélec *et al.* 2007; Shen *et al.* 2008; Huang *et al.* 2009; Zhao *et al.* 2009). High Mn concentrations can be ascribed to meteroic and/or burial diagenesis (Kaufman & Knoll 1995; Jacobsen & Kaufman 1999; Derry 2010), but existing data show that most Neoproterozoic carbonate rocks have relatively lower Fe and Mn concentrations ($<$1000 ppm) and larger local variations than cap carbonates (Yoshioka *et al.* 2003; Frimmel 2008; Zhao *et al.* 2009). Recent studies have indicated that the deep water masses were sometimes sulphidic but were mainly ferruginous (Fe^{2+}-enriched) during the Neoproterozoic (Canfield *et al.* 2008; Li *et al.* 2010). The presence of banded iron formation (BIF) and Mn oxide or carbonate beds in some Cryogenian successions (Klein & Ladeira 2004; Roy 2006; Ilyin 2009; Feng *et al.* 2010) also suggests Fe^{2+}- and Mn^{2+}-enriched seawater. This oceanic chemical condition may have caused the high Fe and Mn concentrations of cap carbonates immediately after Cryogenian glaciations.

In this study, we report element data, including REE, from the outer shelf and basinal sections of the Doushantuo cap carbonate (*c*. 635 Ma) in South China and discuss the potential origin of high Fe and Mn concentrations in the Doushantuo cap carbonate. The results may aid our understanding of the ocean redox conditions at the end of the Nantuo glaciation.

Geological setting

The 3–6 m thick Doushantuo cap carbonate constitutes the base of the Doushantuo Formation, which was inferred to have been deposited on a passive continental margin along the southeastern side of the Yangtze Block (Wang & Li 2003; Jiang *et al.* 2006*a*; Zhou & Xiao 2007). This cap carbonate overlies the glacial diamictites of the Nantuo Formation and forms a regionally consistent stratigraphic marker that extends for more than 350 km from the shelf to the basin (Jiang *et al.* 2003*b*, 2006*a*,*b*) (Figs 1 and 2). The Doushantuo cap carbonate separates the Cryogenian glaciogenic rocks from Ediacaran carbonates and shale, and has been dated at *c*. 635 Ma (Chu *et al.* 2005; Condon *et al.* 2005; Yin *et al.* 2005; Zhang *et al.* 2005).

The Doushantuo cap carbonate mainly consists of micritic and/or microcrystalline dolostone and limestone, with localized bedding disruption, brecciation and cementation at the base (C1 in Fig. 2), which have been interpreted as methane seeps (Jiang *et al.* 2003*a*, 2006*a*,*b*; Wang *et al.* 2008). The general lack of coarse-grained lithology and cross-stratifications and the presence of parallel lamination and graded bedding in the Doushantuo cap carbonate suggest deposition mostly below fair-weather wave base (Jiang *et al.* 2006*a*).

In this study, we focused on two carefully selected sections on

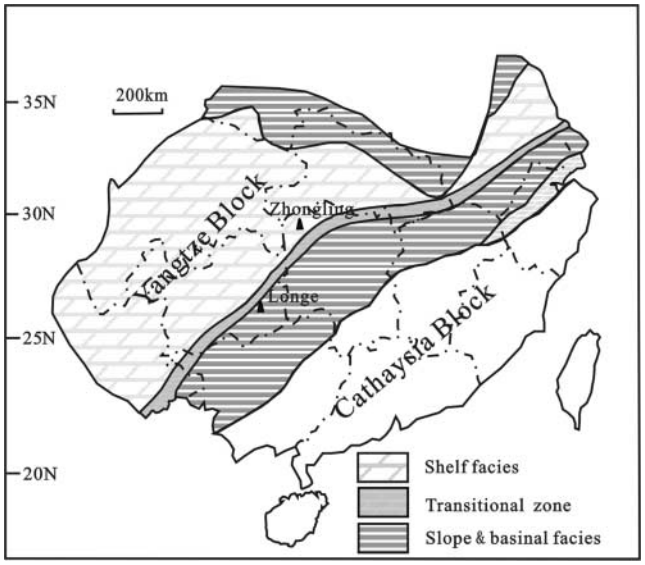

Fig. 1. Simplified palaeogeographical reconstruction of the Ediacaran Yangtze platform in South China showing location of measured cap carbonate sections.

the basis of palaeogeographical location, exposure and availability of fresh samples. The Zhongling section in Hunan province represents the outer-shelf facies and the Longe section in Guizhou Province of China represents the basinal facies (Figs 1 and 2). The Doushantuo cap carbonate in the Zhongling section can be divided into three parts (Fig. 2). The base of the cap carbonate (C1) consists of cliff-forming, buff- to yellow-weathering microcrystalline dolomite with localized bedding disruption, brecciation, cavities and early cementation, similar to features that have been interpreted as methane seeps (Kennedy *et al.* 2001; Jiang *et al.* 2003*a*,*b*). The middle part of cap carbonate (C2) is laminated with local tepee-like structures. The uppermost part of the cap carbonate (C3) consists of thinly laminated, silty and shaly dolostone and limestone. In the Longe section, the cap carbonate is composed of mainly two parts (Fig. 2), the lower cliff-forming, microcrystalline dolostone (C1) and the upper shaly–silty dolostone (C2 + C3).

Methods

All the carbonates were collected at outcrop as large hand samples to ensure sufficient quantity for geochemical analysis. After removing weathered surfaces and secondary veins, the samples were ground to powder (<200 mesh) in an agate mortar for geochemical analysis.

Major elements of bulk samples were analysed by X-ray fluorescence spectrometry (XRF) on a Shimadzu XRF-1500 system using fusion glasses made from a mixture of sample powder and flux ($Li_2B_4O_7$) in the proportion 1:5 at State Key Laboratory of Lithospheric Evolution, Institute of Geology and Geophysics, Chinese Academy of Sciences. The analytical precision monitored by an internal standard is better than 10% (1σ).

For trace elemental analyses, 40 mg of sample powders were reacted with 1 ml of 3M acetic acid in a Teflon pot for 12 h and then centrifuged. Insoluble residues were then removed by filtration, dried and reweighed. The supernatant was dried and re-dissolved in 0.5 ml of 0.1M HNO_3, and dried again. This process was repeated until all acetic acid was removed. The sample was then dissolved in 1% HNO_3. Monitored by an internal standard, In, the final solutions were analysed for trace element, including REE, concentrations by inductively coupled plasma mass spectrometry (ICP-MS) using a Finnigan MAT Element system at State Key Laboratory of Lithospheric Evolution, Institute of Geology and Geophysics, Chinese Academy of Sciences. The analytical precisions monitored by the internal standard are better than 10% (1σ) for trace elements.

A few elements, including Ti, Mn and Fe, were analysed by both XRF and ICP-MS. To distinguish the different methods, we use X_T to represent the XRF results and X_{HAc} to represent the ICP-MS results in the discussion.

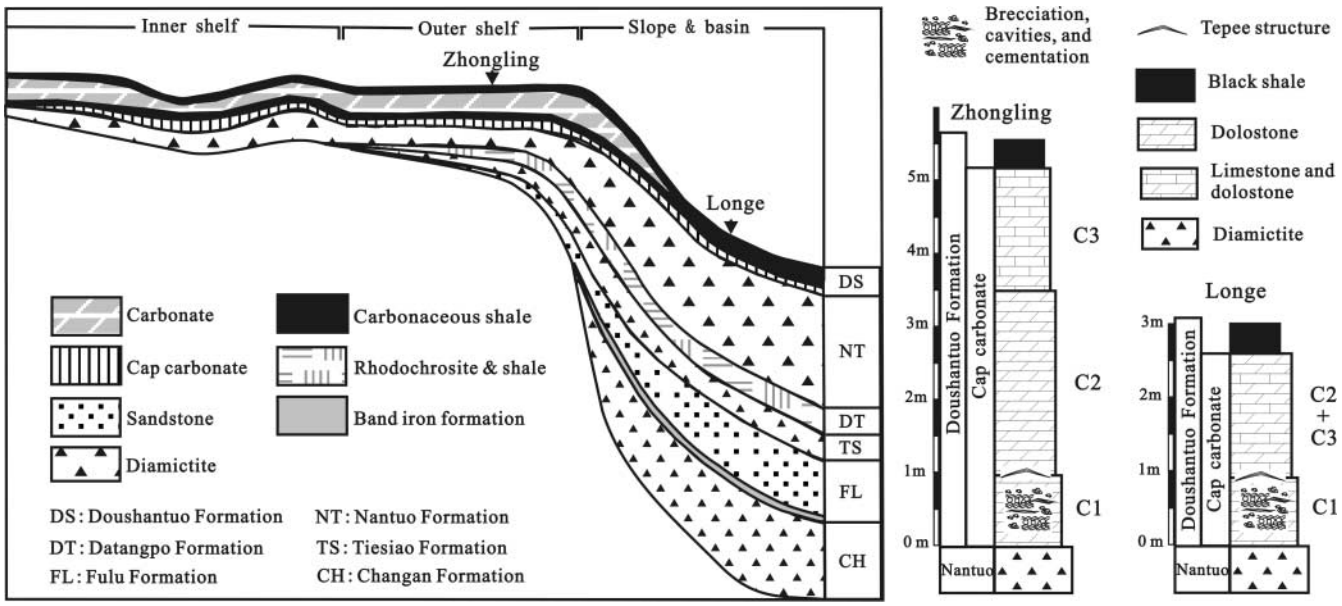

Fig. 2. Neoproterozoic platform–basin transects in South China showing the stratigraphic occurrence of the Doushantuo cap carbonate, location of measured sections, and stratigraphy of the Doushantuo cap carbonate in the Zhongling and Longe sections.

Results

Major elements

Major elements of cap carbonates of the Zhongling and Longe sections are listed in Tables 1 and 2 respectively. Bulk sample MgO contents (*c*. 16–20% in Zhongling section and *c*. 21% in Longe section) and CaO contents (*c*. 27–30% in Zhongling section and *c*. 29% in Longe section) confirm that the carbonates consist mainly of dolomite or Ca-dolomite. All elements of typical detrital origin (SiO_2, TiO_2 and Al_2O_3) have low values, indicating limited detrital sediments in cap carbonates. The outer shelf section (Zhongling; SiO_2 4.7–12.7%; Al_2O_3 0.6–4.2%) has slightly higher SiO_2 and Al_2O_3 contents than the basinal section (Longe; SiO_2 1.8–3.9%; Al_2O_3 0.5–0.9%). These results are consistent with the palaeogeographical reconstruction, in which the Zhongling section was closer to the coastline than the Longe section.

Trace elements and REE

Trace elemental data of the Doushantuo cap carbonate in Zhongling and Longe sections are listed in Tables 3 and 4, respectively. REE anomalies are calculated by the following formulae: $Ce/Ce^* = Ce_N/[Pr_N \times (Pr_N/Nd_N)]$; $Eu/Eu^* = Eu_N/(Sm_N^2 \times Tb_N)^{1/3}$; $La/La^* = La_N/[Pr_N \times (Pr_N/Nd_N)^2]$ (Lawrence *et al.* 2006). Elements with subscript N represent the concentration normalized to Post-Archaean Australian Shale (PAAS) (McLennan 1989).

In both Zhongling and Longe sections, some incompatible elements and high field strength elements (HFSE), such as Zr, Sc and Th, have very low concentrations compared with their concentrations in PAAS. In contrast, most redox-sensitive elements, such as Cr, Mn, Ni, Zn, Mo and Ba, have relatively high concentrations that are close to or higher than those of PAAS.

The cap carbonates in both Zhongling and Longe sections show consistent REE + Y patterns. In the Zhongling section, total REE contents are mostly below 20 ppm ($\Sigma REE = 13.0 \pm 4.4$ ppm), with slightly positive La anomalies ($La/La^* = 0.95 \pm 0.11$), negative Ce anomalies ($Ce/Ce^* = 0.79 \pm 0.06$), positive Y anomalies ($Y_N/Ho_N = 1.15 \pm 0.17$), positive Eu anomalies ($Eu/Eu^* = 1.70 \pm 0.26$), light REE (LREE) depletion and HREE enrichment ($Pr_N/Sm_N = 0.79 \pm 0.06$, $Sm_N/Yb_N = 0.86 \pm 0.25$, $Pr_N/Yb_N = 0.67 \pm 0.19$). In the Longe section, total REE contents are mostly below 10 ppm ($\Sigma REE = 7.8 \pm 2.5$ ppm), with no or slightly positive La anomalies ($La/La^* = 1.05 \pm 0.15$), negative Ce anomalies ($Ce/Ce^* = 0.89 \pm 0.11$), positive Y anomalies ($Y_N/Ho_N = 1.27 \pm 0.16$), distinct positive Eu anomalies

Table 1. *Major element contents of the Doushantuo cap carbonate from the Zhongling section (%)*

Sample:	ZLF1	ZLF5	ZLF8	ZLF9	ZLF10	ZLF11	ZLF14	ZLF16	ZLF18	ZLF20
Depth (m):	0	0.5	0.9	1.2	1.4	1.6	2.6	3.45	4.2	5.2
SiO_2	6.49	10.33	4.71	4.95	7.98	6.59	6.35	5.76	12.66	12.67
TiO_2	0.04	0.23	0.05	0.05	0.06	0.06	0.04	0.06	0.06	0.04
Al_2O_3	0.72	4.23	0.91	1.07	1.33	1.18	0.55	1.1	0.89	1.17
$Fe_2O_3^T$	0.45	1.15	0.65	0.9	0.71	0.6	0.35	0.45	1.47	1.27
MnO	0.19	0.26	0.4	0.62	0.33	0.22	0.14	0.12	0.75	0.66
MgO	19.6	16.18	18.76	18.99	17.32	19.92	19.9	19.85	17	16.5
CaO	29.54	25.64	30.53	29.85	29.95	28.35	29.26	29.15	27.22	27.74
Na_2O	0.11	0.16	0.12	0.01	0.02	0.14	0.01	0.08	0.04	b.d.l.
K_2O	0.19	1.8	0.24	0.26	0.42	0.33	0.21	0.39	0.29	0.52
P_2O_5	0.05	0.09	0.05	0.06	0.07	0.09	0.12	0.11	0.26	0.15
LOI	43.09	37.43	43.48	43.10	41.22	42.65	43.04	42.91	39.21	39.09
Sum	100.47	97.50	99.90	99.86	99.41	100.13	99.97	99.98	99.85	99.81
Fe_T/Al	0.83	0.36	0.94	1.11	0.71	0.67	0.84	0.54	2.18	1.44
Mn_T/Al	0.39	0.09	0.64	0.85	0.36	0.27	0.37	0.16	1.23	0.83

b.d.l., below detection limit.

Table 2. *Major element contents of the Doushantuo cap carbonate from the Longe section (%)*

Sample:	06LEUP01	06LEUP04	06LEUP05	06LEUP06	06LEUP07	06LEUP08	06LEUP09	06LEUP12
Depth (m):	0.2	0.8	1.0	1.2	1.4	1.6	1.8	2.4
SiO_2	2.12	2.65	2.53	3.87	3.06	3.21	2.02	1.82
TiO_2	0.03	0.05	0.05	0.07	0.07	0.06	0.05	0.05
Al_2O_3	0.56	0.89	0.84	0.66	0.68	0.63	0.49	0.69
$Fe_2O_3^T$	1.06	0.74	0.66	0.7	0.87	0.67	0.52	0.7
MnO	1.17	0.2	0.18	0.18	0.42	0.39	0.23	0.35
MgO	21.3	21.77	21.82	21.29	20.94	21.39	21.76	21.68
CaO	29.16	29.26	29.05	28.83	28.77	29	29.61	29.61
Na_2O	b.d.l.	b.d.l.	b.d.l.	0.01	0.26	b.d.l.	b.d.l.	b.d.l.
K_2O	0.08	0.11	0.09	0.08	0.11	0.1	0.09	0.08
P_2O_5	0.05	0.2	0.14	0.14	0.24	0.1	0.09	0.22
LOI	44.34	44.81	44.81	44.50	44.00	44.24	45.10	45.02
Sum	99.87	100.68	100.17	100.33	99.42	99.79	99.96	100.22
Fe_T/Al	2.50	1.10	1.04	1.40	1.69	1.41	1.40	1.34
Mn_T/Al	3.06	0.33	0.31	0.40	0.90	0.91	0.69	0.74

b.d.l., below detection limit.

Table 3. *Trace element, including REE, contents of the Doushantuo cap carbonate from the Zhongling section (ppm)*

Sample:	ZLF1	ZLF4	ZLF5	ZLF8	ZLF9	ZLF10	ZLF11	ZLF14	ZLF16	ZLF18	ZLF20
Depth (m):	0	0.23	0.5	0.9	1.2	1.4	1.6	2.6	3.45	4.2	5.2
Sc	0.64	1.65	3.42	0.92	0.94	1.04	1.08	0.49	0.94	0.79	0.78
Ti	5.90	4.28	3.63	4.38	2.17	5.75	6.57	4.93	5.68	1.37	2.56
V	6.63	1.58	5.19	2.79	2.58	1.84	3.49	9.01	4.07	6.64	11.43
Cr	1665	63	70	77	76	84	79	74	86	112	83
Mn	1860	2322	2500	3227	5071	2811	1762	1085	995	5969	5307
Fe	9093	3704	4137	3939	5785	4077	3713	2746	3005	8853	8454
Co	17.87	2.40	4.24	2.29	2.14	2.12	1.78	1.59	1.69	2.32	2.02
Ni	1088	55	62	58	57	66	60	53	65	78	58
Zn	4222	381	398	363	341	373	360	333	396	429	397
Sr	322	377	528	357	238	267	401	716	411	493	951
Y	0.98	5.63	7.25	3.32	2.45	2.95	4.75	1.77	4.82	3.16	5.36
Zr	1.77	1.11	2.64	1.05	0.56	0.66	0.55	0.25	0.44	0.27	0.36
Mo	196.6	3.4	b.d.l	.5.7	4.0	8.7	6.6	6.1	7.5	8.3	5.9
Cd	2.02	1.51	2.05	0.50	0.29	0.25	0.53	0.84	0.84	0.27	0.50
Cs	0.01	0.01	0.01	0.01	0.00	0.01	0.01	0.01	0.01	0.01	0.01
Ba	94	207	232	145	268	261	175	137	152	207	230
Pb	5.95	7.45	13.82	2.14	1.10	0.38	2.30	0.71	3.26	1.41	3.11
Th	0.02	0.38	0.76	0.25	0.22	0.28	0.25	0.11	0.27	0.10	0.15
U	0.30	0.24	0.31	0.31	0.17	0.30	0.20	0.15	0.27	0.20	0.23
La	0.97	3.99	4.23	2.94	2.10	2.73	2.67	1.77	3.02	2.27	3.28
Ce	1.63	6.92	7.11	5.25	4.31	5.96	3.99	2.95	4.08	3.62	5.05
Pr	0.24	0.88	0.96	0.68	0.54	0.76	0.62	0.37	0.60	0.47	0.74
Nd	0.96	3.21	3.60	2.44	2.02	2.87	2.37	1.40	2.34	1.59	2.67
Sm	0.19	0.66	0.75	0.52	0.42	0.64	0.56	0.30	0.53	0.33	0.57
Eu	0.09	0.20	0.23	0.16	0.17	0.21	0.18	0.12	0.17	0.13	0.21
Gd	0.20	0.68	0.79	0.50	0.40	0.57	0.66	0.32	0.61	0.39	0.66
Tb	0.03	0.11	0.14	0.08	0.07	0.09	0.11	0.05	0.11	0.07	0.12
Dy	0.20	0.67	0.89	0.50	0.38	0.50	0.69	0.29	0.70	0.42	0.75
Ho	0.05	0.15	0.20	0.11	0.08	0.10	0.15	0.06	0.15	0.09	0.16
Er	0.14	0.44	0.59	0.31	0.24	0.26	0.42	0.16	0.42	0.27	0.45
Tm	0.02	0.07	0.09	0.05	0.04	0.04	0.06	0.02	0.06	0.04	0.07
Yb	0.13	0.44	0.61	0.30	0.23	0.22	0.38	0.13	0.37	0.24	0.39
Lu	0.02	0.07	0.10	0.05	0.04	0.03	0.06	0.02	0.05	0.04	0.05
Ce/Ce*	0.79	0.82	0.80	0.80	0.86	0.85	0.71	0.86	0.77	0.75	0.70
Eu/Eu*	2.23	1.51	1.45	1.53	2.04	1.72	1.50	1.87	1.41	1.75	1.66
La/La*	1.03	0.94	0.97	0.88	0.85	0.79	0.97	1.05	1.20	0.86	0.89
Pr_N/Sm_N	0.78	0.85	0.81	0.81	0.82	0.75	0.70	0.77	0.71	0.90	0.82
Sm_N/Yb_N	0.75	0.76	0.62	0.88	0.91	1.47	0.74	1.20	0.73	0.68	0.74
Pr_N/Yb_N	0.58	0.65	0.50	0.71	0.74	1.10	0.52	0.93	0.51	0.62	0.61
Y_N/Ho_N	0.76	1.40	1.35	1.13	1.07	1.06	1.17	1.10	1.17	1.25	1.21
$\sum$REE	4.87	18.49	20.29	13.91	11.04	14.99	12.91	7.96	13.21	9.96	15.16

(Eu/Eu* $= 2.29 \pm 0.76$), LREE depletion and HREE enrichment ($Pr_N/Sm_N = 0.54 \pm 0.12$, $Sm_N/Yb_N = 0.63 \pm 0.11$, $Pr_N/Yb_N = 0.34 \pm 0.09$).

Discussion

Fidelity of trace elements and REE

Zhao *et al.* (2009) analysed trace elements of Ediacaran carbonates by stepwise dissolution with different strengths of acid. They found that calcite was principally dissolved in 0.5M acetic acid, and dolomite was principally dissolved in 3.4M acetic acid. In this study, 3M acetic acid was used for trace elemental analysis, which can dissolve most calcite and dolomite in the cap carbonates. TiO_2 content range is *c.* 0.03–0.07% (i.e. *c.* 180–420 ppm of Ti_T) in bulk samples, whereas the Ti_{HAc} range is *c.* 1–7 ppm by acetic acid solution, which indicated that acetic acid dissolution is very effective in removing detrital impact.

Some incompatible elements and HFSE (e.g. Zr, Th and Sc) commonly have been used to track detritus from continents (Calvert & Pedersen 1993; Tribovillard *et al.* 1994; Hild & Brumsack 1998; Böing *et al.* 2004). For the trace elements dissolved by acetic acid, very low concentrations of Zr, Th and Sc (in comparison with PAAS) indicate negligible detrital contributions. There is no correlation between Zr and redox-sensitive elements (e.g. Fe, Mn and Ba) in both Zhongling and Longe sections (Fig. 3), indicating that detrital contributions to redox-sensitive elements are trivial. The lack of correlation between Zr and total REE contents also indicates that detrital contribution to REE is negligible (Fig. 3). In addition, the total REE contents are in the typical range of marine carbonates (Webb & Kamber 2000; Nothdurft *et al.* 2004), which also indicates minor detrital contributions.

Trace elements are sensitive to palaeoenvironmental conditions and to diagenetic alteration during diagenesis. High Mn contents together with Mn/Sr > 2 are commonly regarded as indicators for diagenetic alteration of limestones, because Sr is commonly expelled from sedimentary carbonates, whereas Mn is incorporated during diagenesis (Jacobsen & Kaufman 1999). High Mn/Sr ratios are observed in our studies, but we consider that the Mn enrichment in cap carbonates is more probably related to the coeval seawater chemistry rather than a diagenetic artefact

Table 4. *Trace element, including REE, contents of the Doushantuo cap carbonate from the Longe section (ppm)*

Sample:	06LEUP01	06LEUP02	06LEUP04	06LEUP05	06LEUP06	06LEUP07	06LEUP08	06LEUP09	06LEUP12
Depth (m):	0.2	0.4	0.8	1.0	1.2	1.4	1.6	1.8	2.4
Sc	0.51	0.31	0.65	0.64	1.06	1.06	1.08	0.58	0.63
Ti	1.76	2.56	2.25	1.67	1.43	4.10	3.84	4.37	2.43
V	17	15	7	7	4	79	63	35	20
Cr	17	749	298	162	25	105	161	38	31
Mn	9029	7195	1614	1397	1304	3430	2909	1745	2485
Fe	3851	6902	4464	4054	3825	5113	3773	2536	3019
Co	2.19	9.24	4.28	2.75	0.94	1.59	2.46	0.97	1.01
Ni	29	552	247	148	23	88	143	39	22
Zn	70	1173	533	362	94	250	436	99	98
Rb	0.44	0.34	0.36	0.30	0.03	0.04	0.65	0.36	0.28
Sr	114	111	94	102	137	253	164	145	162
Y	3.23	2.07	5.59	4.40	4.19	9.44	3.25	2.15	4.59
Zr	0.61	1.11	0.90	0.92	0.51	1.74	1.02	0.71	0.58
Mo	b.d.l.	93	24	11	b.d.l.	10	15	1	b.d.l.
Cd	0.17	0.47	0.17	0.12	0.28	0.07	0.04	0.01	0.03
Ba	194	74	210	290	354	668	682	351	364
Pb	2.75	2.57	2.25	71.16	1.92	0.42	0.23	0.69	0.76
Th	0.15	0.06	0.10	0.15	0.20	0.27	0.20	0.26	0.33
U	0.34	0.22	0.21	0.18	0.09	1.23	1.90	2.63	2.83
La	1.23	0.81	1.02	1.45	1.58	1.64	0.94	0.86	1.12
Ce	2.59	1.63	1.67	2.41	3.32	3.06	1.77	1.79	2.34
Pr	0.31	0.20	0.31	0.41	0.46	0.47	0.25	0.21	0.27
Nd	1.20	0.73	1.49	2.00	1.87	2.10	1.04	0.84	1.15
Sm	0.31	0.18	0.58	0.63	0.48	0.68	0.27	0.21	0.30
Eu	0.14	0.07	0.21	0.23	0.19	0.33	0.24	0.14	0.18
Gd	0.37	0.23	0.76	0.71	0.50	0.92	0.31	0.22	0.39
Tb	0.06	0.04	0.15	0.12	0.09	0.16	0.06	0.04	0.07
Dy	0.42	0.27	0.92	0.74	0.54	1.11	0.41	0.26	0.47
Ho	0.09	0.06	0.21	0.16	0.12	0.25	0.09	0.06	0.11
Er	0.27	0.17	0.57	0.43	0.33	0.70	0.27	0.17	0.33
Tm	0.04	0.02	0.09	0.06	0.05	0.10	0.04	0.03	0.05
Yb	0.28	0.15	0.55	0.40	0.30	0.57	0.26	0.16	0.25
Lu	0.04	0.02	0.08	0.06	0.04	0.08	0.04	0.02	0.03
Ce/Ce*	0.94	0.87	0.73	0.82	0.85	0.84	0.82	1.00	1.10
Eu/Eu*	2.10	1.81	1.54	1.66	1.91	2.06	3.87	3.12	2.54
La/La*	0.94	0.87	1.14	1.29	0.89	1.08	0.97	1.04	1.24
Pr_N/Sm_N	0.64	0.70	0.34	0.41	0.60	0.44	0.59	0.61	0.56
Sm_N/Yb_N	0.56	0.59	0.53	0.81	0.80	0.60	0.54	0.70	0.62
Pr_N/Yb_N	0.36	0.42	0.18	0.33	0.49	0.26	0.32	0.43	0.35
Y_N/Ho_N	1.28	1.31	0.98	1.04	1.33	1.40	1.27	1.35	1.49
$\sum$REE	7.35	4.60	8.61	9.82	9.87	12.17	5.98	5.02	7.06

Elements with subscript N represent the concentration normalized to Post-Archaean Australian Shale (PAAS) (McLennan 1989). REE anomalies are calculated by the following formulae (Lawrence *et al.* 2006): $Ce/Ce^* = Ce_N/[Pr_N \times (Pr_N/Nd_N)]$; $Eu/Eu^* = Eu_N/(Sm_N^2 \times Tb_N)^{1/3}$; $La/La^* = La_N/[Pr_N \times (Pr_N/Nd_N)^2]$.

because Mn concentrations mimic those of other redox-sensitive elements (Figs 4 and 5). This is consistent with earlier studies that show high Mn concentrations in other time-equivalent cap carbonates, which were interpreted as resulting from anoxic or suboxic depositional environments (Shen *et al.* 2005; Font *et al.* 2006; Hurtgen *et al.* 2006; Nédélec *et al.* 2007; Feng *et al.* 2010). Similarly, high Mn/Sr ratios also have been reported from the early Cryogenian cap carbonates and interpreted as recording unusual seawater composition (Yoshioka *et al.* 2003).

REE + Y replace Ca^{2+} in carbonate lattices and can remain stable for a long geological time (Zhong & Mucci 1995). Once REE are set in a stable carbonate lattice, solid-state diffusion is minimal even at metamorphic temperatures (Cherniak 1998). Most diagenetic fluids contain very low REE + Y (10^{-6} to 10^{-4} ppm) and would have very limited influence on the REE + Y of carbonate rocks (Sholkovitz *et al.* 1989; Banner & Hanson 1990). Furthermore, calcite cement formation can strongly reduce the permeability and porosity of sedimentary carbonates, which stops REE + Y incorporation from seawater during early diagenesis (Tanaka & Kawabe 2006). Many well-constrained diagenetic studies suggest that REE + Y patterns were very stable in ancient carbonates that underwent diagenesis (Webb & Kamber 2000; Nothdurft *et al.* 2004; Webb *et al.* 2009).

Banner *et al.* (1988) found that extensive early dolomitization of Carboniferous marine limestones in seawater-dominated fluid did not alter marine REE + Y patterns, and a subsequent phase of dolomitization in non-marine fluids that caused major textual recrystallization and compositional change likewise did not alter REE patterns either. Webb *et al.* (2009) also noted that many ancient dolomites might preserve intact seawater REE + Y proxies.

In summary, the lack of detrital contribution to trace elements and REE + Y patterns, the covariation of Mn and redox-sensitive elements, and the similarity of results between the Doushantuo cap carbonate and other time-equivalent cap carbonates argue that the trace elements and REE of the Doushantuo cap carbonate probably record the coeval seawater composition from

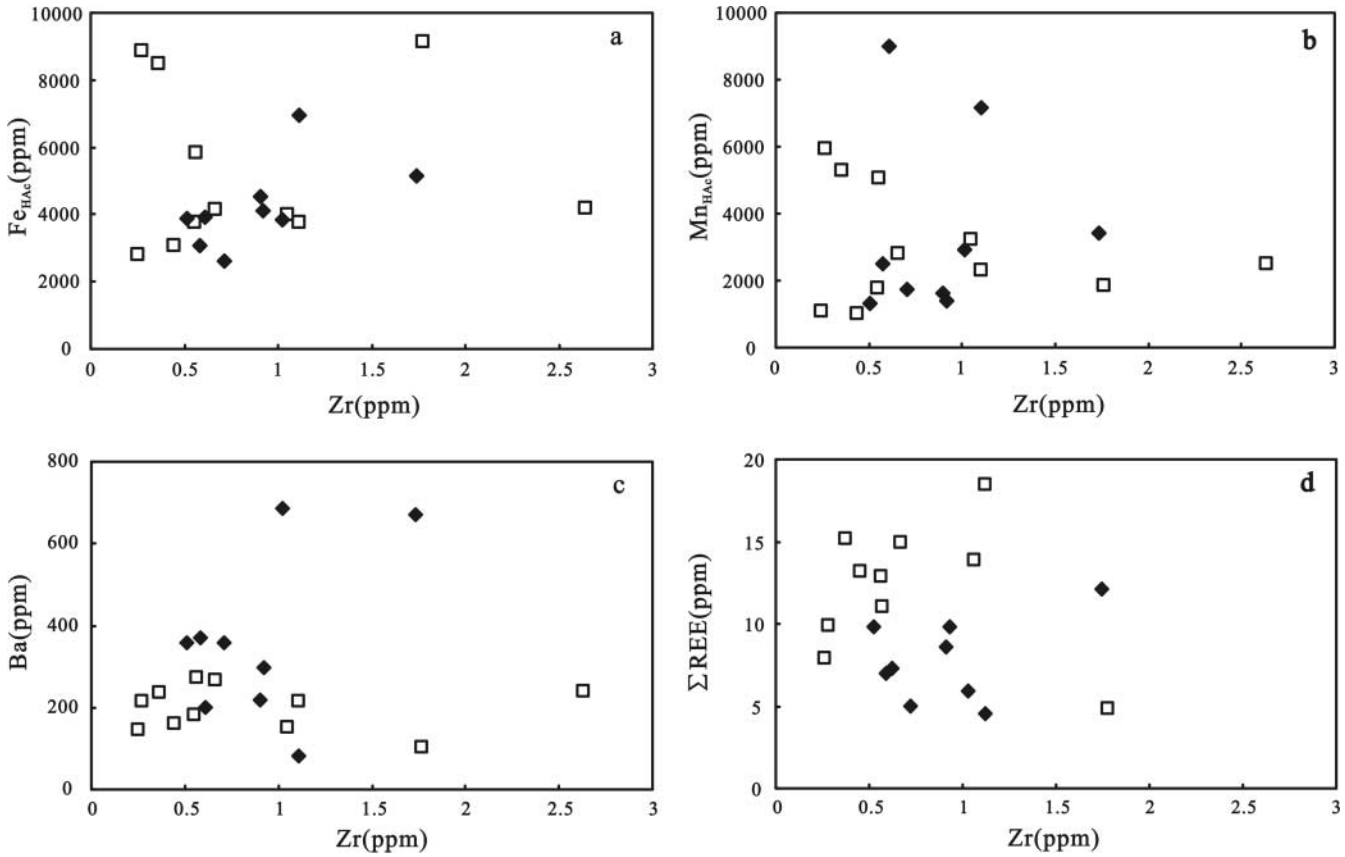

Fig. 3. Correlations between Zr and Fe, Mn, Ba and ∑REE. Open squares are samples from the Zhongling section; filled rhombuses are samples from the Longe section.

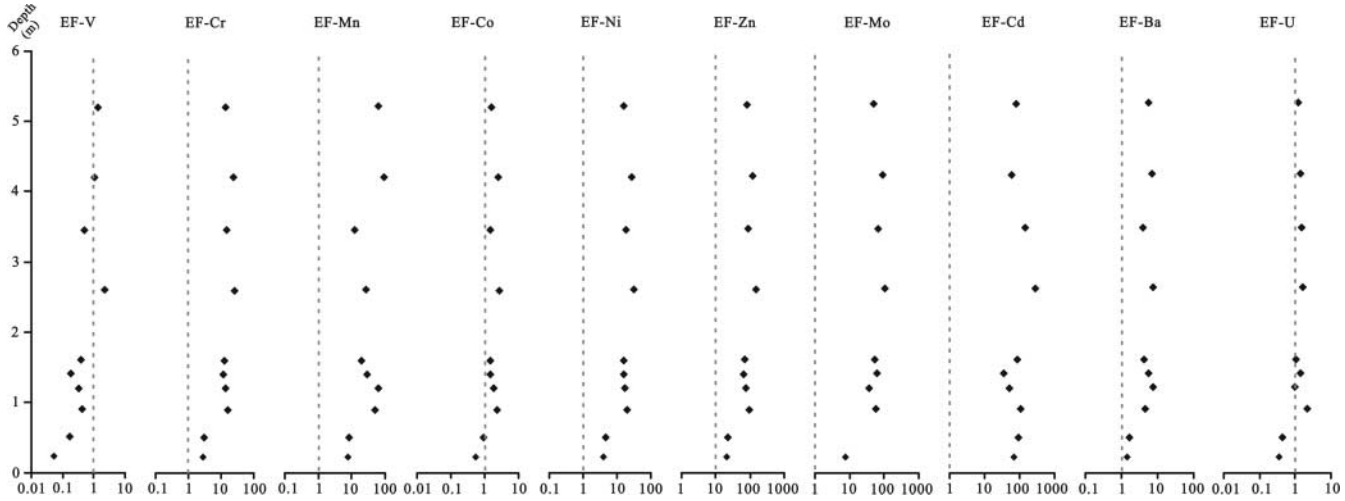

Fig. 4. Enrichment factor (EF) of redox-sensitive elements of the Doushantuo cap carbonate from the Zhongling section.

which the cap carbonates were precipitated rather than diagenetic artefacts.

Redox conditions during cap carbonate deposition

Redox-sensitive elements, such as V, U, Co, Ni, Zn and Cd, can be used to track the redox conditions of depositional environments (Morford & Emerson 1999; Morford *et al.* 2001; Tribovillard *et al.* 2006). The enrichment factors (EF) of redox-sensitive trace elements are commonly used to estimate if these elements are relatively enriched or depleted: EF-$X_{element}$ = $(X_T/Al_T)/(X_{PAAS}/Al_{PAAS})$ (Tribovillard *et al.* 2006). In this study, the concentrations of trace elements were analysed through acetic acid dissolution, and their values (X_{HAc}) should be lower than

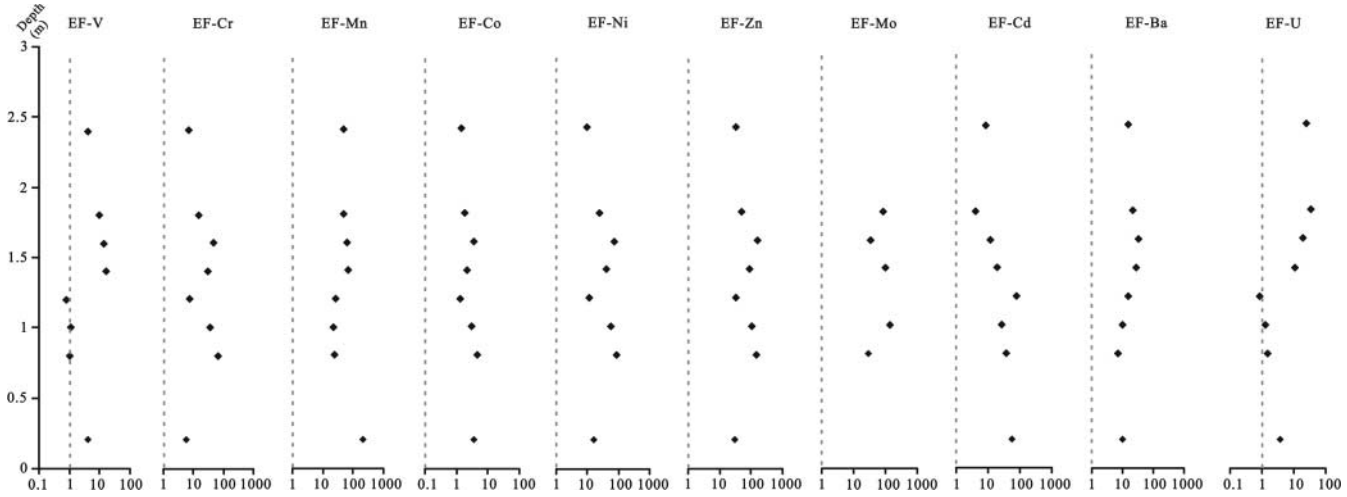

Fig. 5. Enrichment factor (EF) of redox-sensitive elements of the Doushantuo cap carbonate from the Longe section.

X_T. The results calculated by EF-$X = (X_{HAc}/Al_T)/(X_{PAAS}/Al_{PAAS})$ would be lower than the real EF-X. Even so, most EF-X values of cap carbonates are much greater than unity (Figs 4 and 5), which indicates that the redox-sensitive elements are enriched relative to PAAS. Elevated EF suggests anoxic conditions during cap carbonate precipitation in both Zhongling and Longe sections. Assuming that cap carbonates were precipitated near the surface ocean (photic zone), as has been suggested by the presence of peloids and stromatolites in the Doushantuo cap carbonate (Jiang *et al.* 2003*a*, 2006*a*) and other cap carbonates globally (e.g. Kennedy 1996; James *et al.* 2001; Nogueira *et al.* 2003; Halverson *et al.* 2004; Xiao *et al.* 2004; Corsetti & Grotzinger 2005; Hoffman *et al.* 2007), enrichment of redox-sensitive elements in both shelf (Zhongling) and basin (Longe) sections imply that seawater anoxia may have reached a shallow water depth within the photic zone.

In the modern ocean, dissolved REE show large negative Ce anomalies (*c*. 0.06–0.16) because of the oxidation and removal of Ce through Mn nodules and Mn–Fe oxides in the oxic water column (Byrne & Sholkovitz 1996). The Ce carried by rivers is precipitated largely in coastal settings. In suboxic and anoxic waters, Ce anomalies are smaller or absent owing to reductive dissolution of settling Mn- and Fe-rich particles (German *et al.* 1991). In anoxic (euxinic) environments such as the Black Sea, the Ce/Ce* values range from about 0.8 to 1.0 (German *et al.* 1991). In this study, most cap carbonate samples show slightly negative Ce anomalies ranging between 0.8 and 1 (Tables 3 and 4), which indicate euxinic or anoxic depositional conditions.

The Fe_T/Al ratio can be used as an independent palaeoredox proxy. Based on the iron shuttle model (Lyons & Severmann 2006), recycled reactive Fe exported from oxic or suboxic shelves would accumulate in euxinic basins where reactive Fe is trapped as iron sulphide. Thus, the Fe_T/Al ratio would be enhanced in euxinic basins (Anderson & Raiswell 2004; Lyons & Severmann 2006). Results from Black Sea sediments (Lyons & Severmann 2006) show that Fe_T/Al ratios (0.5–0.6) of oxic sediments are significantly lower than those of euxinic sediments (0.6–1.2). Most Fe_T/Al ratios of the cap carbonates in the Zhongling section are >0.6, and those from the Longe section are >1 (Tables 1 and 2). However, in the Black Sea sediments there are strong Fe_T–Al and Mn_T–Al correlations in both oxic shelf and euxinic basinal environments (Lyons & Severmann 2006), implying that the enrichment of Fe and Mn in the basin was due to the transportation of recycled Fe and Mn from shelf to basinal environments (the 'iron shuttle'). In the Doushantuo cap carbonate, no Fe_T–Al and Mn_T–Al correlations have been observed in both outer shelf and basinal sections (Fig. 6). This indicates that the enrichment of Fe and Mn in the Doushantuo cap carbonate was not through an iron or manganese shuttle.

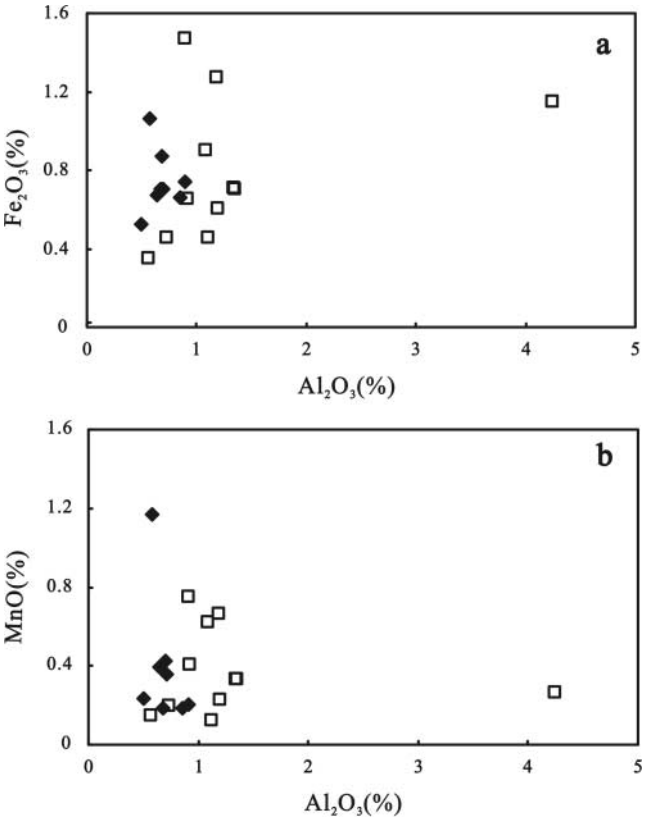

Fig. 6. Cross-plots of Al_2O_3–Fe_2O_3 and Al_2O_3–MnO. Open squares are samples from the Zhongling section; filled rhombuses are samples from the Longe section.

For most of the measured samples, the Fe_{HAc} value is very close to the Fe_T value, and the Mn_{HAc} value is nearly identical to the Mn_T value within analytical uncertainties (Fig. 7). This suggests that Fe^{2+} and Mn^{2+} were incorporated into the lattices of carbonate and replaced Ca^{2+} and Mg^{2+} ions during cap carbonate precipitation. This is consistent with the fact that there was almost no extractable pyrite sulphur from our samples by reduced chloride solution. In combination with the enrichment of redox-sensitive elements in samples, it implies that the depositional environment was anoxic and ferruginous (Fe^{2+}-enriched) but not euxinic because, if the seawater was euxinic, Fe^{2+} and other metal ions would prefer to precipitate as sulphides, such as pyrite.

Sources of REE and iron in cap carbonates

HREE enrichment and positive Y anomalies of the Doushantuo cap carbonate are similar to those of modern seawater, but the positive Eu anomalies require more specific conditions (Fig. 8). In modern hydrothermal systems at mid-ocean ridges, Eu^{3+} is reduced to Eu^{2+} during alteration of mid-ocean ridge basalt (MORB). As a result of reduced sorption of Eu^{2+} (rather than Eu^{3+}), the discharging fluids are enriched in total Eu (German *et al.* 1993; Edmonds & German 2004; Chavagnac *et al.* 2005). Thus, positive Eu anomalies are associated with reduced, high-temperature hydrothermal fluids.

Positive Eu anomalies have been found in other deep-water sections of the Doushantuo cap carbonate (Zhao *et al.* 2009) and in other time-equivalent cap carbonates in Ghana (Nédélec *et al.* 2007). The widespread occurrence of positive Eu anomalies in deep-water cap carbonates suggests that they were not the result of localized hydrothermal vents but probably represent mixed seawater

In the modern ocean, hydrothermally injected REE do not influence the REE budget of seawater because injected REE are scavenged by precipitating hydroxides. However, in the early oceans, oxygen in deep oceans was deficient, and riverine sulphate input was very low, leading to anoxic conditions with very limited H_2S in deep water (Canfield & Raiswell 1999; Canfield 2004). This condition was capable of keeping Fe^{2+} and Mn^{2+} in solution and prevented stripping of REE. Hydrothermal solutions were considered as the main source of REE in deep water during the Archaean and Palaeoproterozoic, when sediments carried a chemical signal from both seawater and hydrothermal fluids (Frei & Dahl 2007; Frei *et al.* 2008). The Doushantuo cap carbonate shows REE+Y patterns (Fig. 8) that are similar to those obtained from Archaean and Palaeoproterozoic chemical sediments (Fig. 9), including HREE enrichment, positive Y anomalies and positive Eu anomalies. These similarities suggest that, during cap carbonate deposition, seawater composition was strongly influenced by hydrothermal solutions from the deep ocean, somewhat like Archaean and Palaeoproterozoic oceans in chemistry.

Global Neoproterozoic glaciations and hydrothermal input were considered to have played important roles in regulating the Neoproterozoic ocean chemistry. Severe glaciations would cause a stagnant and anoxic ocean (Kirschvink 1992), and the frozen surface would attenuate the flux of reduced sulphur (Canfield & Raiswell 1999). Prolonged input of hydrothermal solutions on the sea floor can be accumulated in the ocean. Through time the chemical composition of seawater would be strongly influenced by hydrothermal solutions on the sea floor, attaining features such as positive Eu anomalies in REE+Y patterns. More importantly, hydrothermal fluids are enriched in some transition metals (e.g. Fe, Mn and Cu), in which Fe is the most enriched (Von Damm 1995; Cruse & Lyons 2004; Edmonds & German

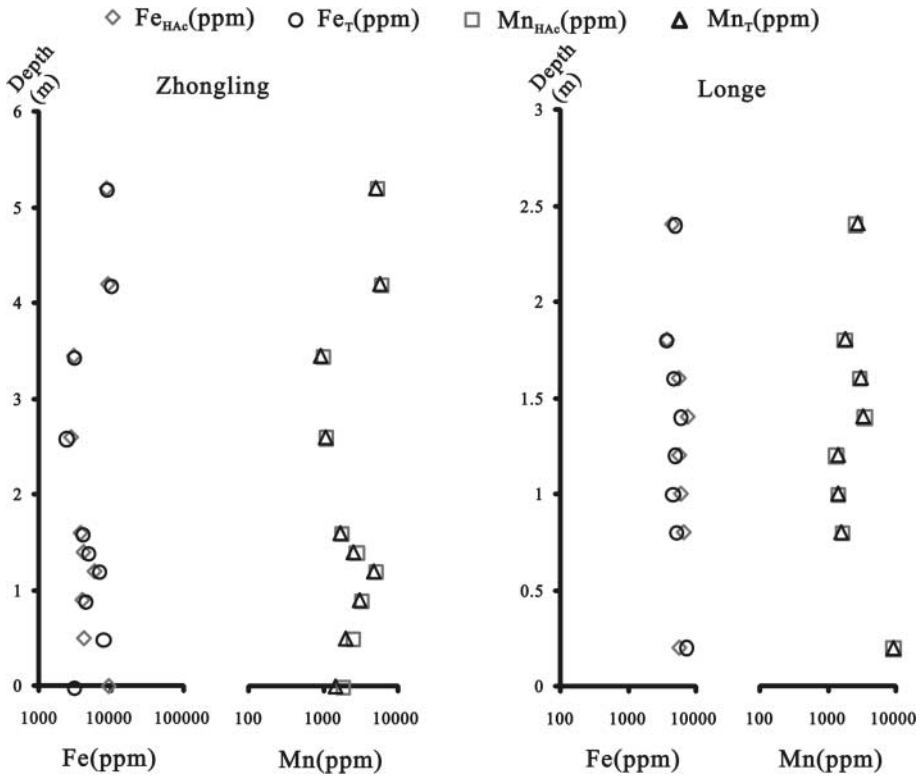

Fig. 7. Comparison between Fe_{HAc} and Fe_T, Mn_{HAc} and Mn_T of the Doushantuo cap carbonate from the Zhongling (left) and Longe (right) sections. Identical Fe_{HAc} and Fe_T, Mn_{HAc} and Mn_T values in both sections suggest that most Fe and Mn are incorporated in lattices of carbonates rather than sulphides.

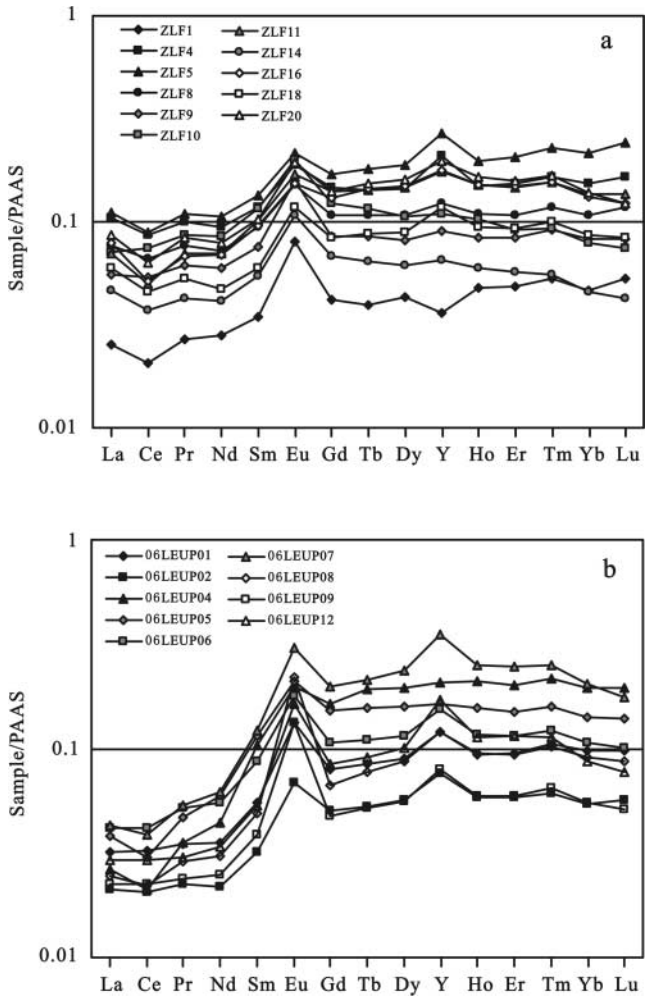

Fig. 8. REE + Y patterns of the Doushantuo cap carbonate from Zhongling (**a**) and Longe (**b**) sections.

2004). In addition, sea-level fall during Neoproterozoic glaciations would significantly elevate the Fe content and Fe/H_2S ratio of mid-ocean ridge hydrothermal fluids (Kump & Seyfried 2005). The input of hydrothermal fluids with high Fe/H_2S ratio would effectively enhance Fe^{2+} concentration in the deep ocean.

It is difficult to confirm that the change of deep ocean from H_2S-enriched to ferruginous during the Neoproterozoic was due to global glaciations and hydrothermal input, because transformation from H_2S-enriched deep ocean to ferruginous has been proposed to occur possibly before the early Cryogenian (Sturtian) glaciation (Johnston *et al.* 2010), and enhanced weathering of basalt before Sturtian glaciation would provide abundant iron to the ocean (Goddéris *et al.* 2003; Donnadieu *et al.* 2004). However, a reasonable conclusion that can be drawn from this study is that the global glaciations and hydrothermal input played a very important role in sustaining the ferruginous deep ocean that may have lasted until the late Ediacaran period, because BIF and rhodochrosite associated with Sturtian glaciation (Klein & Ladeira 2004; Klein 2005; Roy 2006; Ilyin 2009; Feng *et al.* 2010) and the Doushantuo cap carbonate after Nantuo glaciation both suggest ferruginous conditions influenced by hydrothermal solutions from deep-ocean seawater.

Conclusion

New results for major elements, trace elements and REE of the Doushantuo cap carbonate (*c*. 635 Ma) deposited in outer-shelf and basinal environments in South China are reported. Enrichment in redox-sensitive elements and slightly negative Ce anomalies in cap carbonates indicate anoxic marine environments during cap carbonate deposition. However, high Fe_T/Al ratios and very low extractable pyrite Fe do not signify euxinic conditions. In combination with results from other time-equivalent cap carbonates, the high Fe and Mn concentrations in the Doushantuo cap carbonate were probably from enriched Fe^{2+} in seawater, implying ferruginous seawater during and after the Nantuo glaciation.

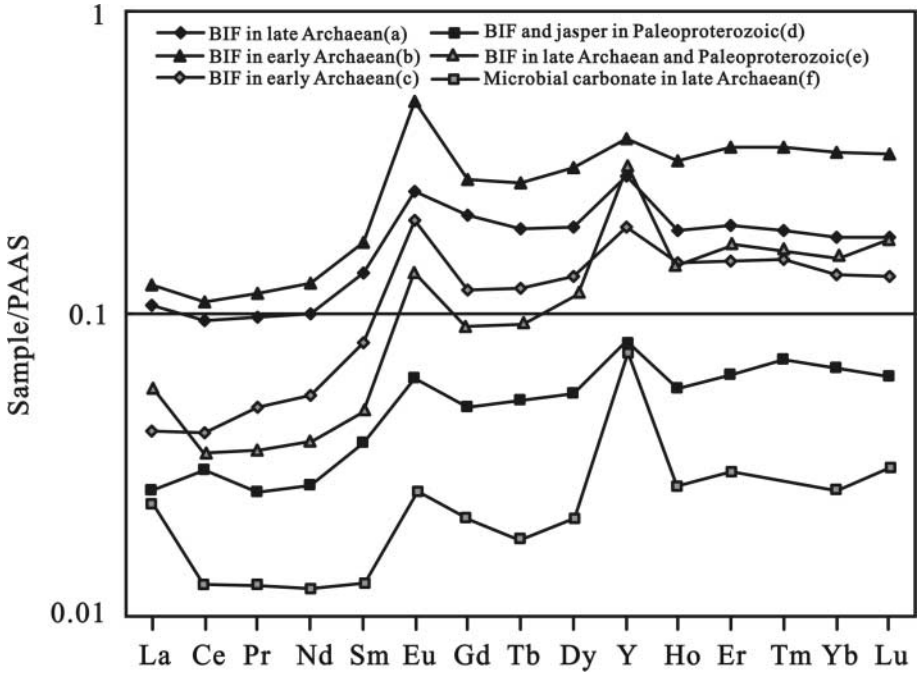

Fig. 9. REE + Y patterns of some Archaean and Palaeoproterozoic chemical sediments. Data source: (**a**, **b**) Frei *et al.* (2008); (**c**) Bolhar *et al.* (2004); (**d**) Slack *et al.* (2007); (**e**) Bau & Dulski (1996); (**f**) Kamber & Webb (2001).

The REE + Y patterns of the Doushantuo cap carbonate show enrichment of HREE, positive Eu anomalies and positive Y anomalies, which were similar to those of the Archaean and Palaeoproterozoic chemical sediments. Similar to Archaean and Palaeoproterozoic oceans whose chemical compositions were strongly influenced by hydrothermal fluids, the high concentration of Fe, Mn and redox-sensitive elements in the Doushantuo cap carbonate may originated from Fe-rich hydrothermal solution in the deep ocean. Ferruginous deep ocean inherited from Cryogenian oceans may have continued through deposition of the cap carbonates, leading to ferruginous conditions in some Ediacaran basins.

This research is funded by the Ministry of Science and Technology of China (Grant 2011CB808805) and the Natural Science Foundation of China (Grants 40532012, 40873007, 40603021). The US National Science Foundation provided support to G.Q.J. (EAR-0745825). We thank X. D. Jin and F. S. Zhang for laboratory assistant. We also thank Q. R. Zhang and H. C. Wu for field work. Finally, we thank journal editor J. Hendry and two anonymous reviewers for their constructive comments, which improved this paper.

References

Anderson, T.F. & Raiswell, R. 2004. Sources and mechanisms for the enrichment of highly reactive iron in euxinic Black Sea sediments. *American Journal of Science*, **304**, 203–233.

Banner, J.L. & Hanson, G.N. 1990. Calculation of simultaneous isotopic and trace element variations during water–rock interaction with applications to carbonate diagenesis. *Geochimica et Cosmochimica Acta*, **54**, 3123–3137.

Banner, J.L., Hanson, G.N. & Meyers, W.J. 1988. Rare earth element and Nd isotopic variations in regionally extensive dolomites from the Burlington–Keokuk Formation (Mississippian): implications for REE mobility during carbonate diagenesis. *Journal of Sedimentary Petrology*, **58**, 415–432.

Bau, M. & Dulski, P. 1996. Distribution of yttrium and rare-earth elements in the Penge and Kuruman iron-formations, Transvaal Supergroup, South Africa. *Precambrian Research*, **79**, 37–55.

Böing, P., Brumsack, H.J., Böttcher, M.E., Schnetger, B., Kriete, C., Kallmeyer, J. & Borchers, S.L. 2004. Geochemistry of Peruvian near-surface sediments. *Geochimica et Cosmochimica Acta*, **68**, 4429–4451.

Bolhar, R., Kamber, B.S., Moorbath, S., Fedo, C.M. & Whitehouse, M.J. 2004. Characterisation of early Archaean chemical sediments by trace element signatures. *Earth and Planetary Science Letters*, **222**, 43–60.

Byrne, R.H. & Sholkovitz, E.R. 1996. Marine chemistry and geochemistry of the lanthanides. *In:* Gschneidner, K.A., Jr & Eyring, L. (eds) *Handbook on the Physics and Chemistry of Rare Earths, Vol. 23*. Elsevier, Amsterdam, 497–593.

Calvert, S.E. & Pedersen, T.F. 1993. Geochemistry of Recent oxic and anoxic marine sediments: Implications for the geological record. *Marine Geology*, **113**, 67–88.

Canfield, D.E. 2004. The evolution of the Earth surface sulfur reservoir. *American Journal of Science*, **304**, 839–861.

Canfield, D.E. & Raiswell, R. 1999. The evolution of the sulfur cycle. *American Journal of Science*, **299**, 697–723.

Canfield, D.E., Poulton, S.W., Knoll, A.H., Narbonne, G.M., Ross, G., Goldberg, T. & Strauss, H. 2008. Ferruginous conditions dominated later Neoproterozoic deep-water chemistry. *Science*, **321**, 949–952.

Chavagnac, V., German, C.R., Milton, J.A. & Palmer, M.R. 2005. Sources of REE in sediment cores from the Rainbow vent site (36°14'N, MAR). *Chemical Geology*, **216**, 329–352.

Cherniak, D.J. 1998. REE diffusion in calcite. *Earth and Planetary Science Letters*, **160**, 273–287.

Chu, X.L., Todt, W., Zhang, Q.R., Chen, F.K. & Huang, J. 2005. U–Pb zircon age for the Nanhua–Sinian boundary. *Chinese Science Bulletin*, **50**, 716–718.

Condon, D., Zhu, M.Y., Bowring, S., Wang, W., Yang, A.H. & Jin, Y.G. 2005. U–Pb ages from the Neoproterozoic Doushantuo Formation, China. *Science*, **308**, 95–98.

Corsetti, F.A. & Grotzinger, J.P. 2005. Origin and significance of tube structures in Neoproterozoic post-glacial cap carbonates: example from Noonday Dolomite, Death Valley, United States. *Palaios*, **20**, 348–362.

Cruse, A.M. & Lyons, T.W. 2004. Trace metal records of regional paleoenvironmental variability in Pennsylvanian (Upper Carboniferous) black shales. *Chemical Geology*, **206**, 319–345.

de Alvarenga, C.J.S., Santos, R.V. & Dantas, E.L. 2004. C–O–Sr isotopic stratigraphy of cap carbonates overlying Marinoan-age glacial diamictites in the Paraguay Belt, Brazil. *Precambrian Research*, **131**, 1–21.

Derry, L.A. 2010. A burial diagenesis origin for the Ediacaran Shuram-Wonoka carbon isotope anomaly. *Earth and Planetary Science Letters*, **294**, 152–162.

Donnadieu, Y., Goddéris, Y., Ramstein, G., Nédélec, A. & Meert, J. 2004. A 'snowball Earth' climate triggered by continental break-up through changes in runoff. *Nature*, **428**, 303–306.

Edmonds, H.N. & German, C.R. 2004. Particle geochemistry in the Rainbow hydrothermal plume, Mid-Atlantic Ridge. *Geochimica et Cosmochimica Acta*, **68**, 759–772.

Fairchild, I.J. & Kennedy, M.J. 2007. Neoproterozoic glaciation in the Earth System. *Journal of the Geological Society, London*, **164**, 895–921.

Feng, L.-J., Chu, X.-L., Huang, J., Zhang, Q.-R. & Chang, H.-J. 2010. Reconstruction of paleo-redox conditions and early sulfur cycling during deposition of the Cryogenian Datangpo Formation in South China, *Gondwana Research*, **18**, 632–637.

Font, E., Nédélec, A., Trindade, R.I.F., Macouin, M. & Charrière, A. 2006. Chemostratigraphy of the Neoproterozoic Mirassol d'Oeste cap dolostones (Mato Grosso, Brazil): An alternative model for Marinoan cap dolostone formation. *Earth and Planetary Science Letters*, **250**, 89–103.

Frei, R. & Dahl, P.S. 2007. Trace element and isotopic characterization of Neoarchean–Paleoproterozoic BIFs (Black Hills, South Dakota, USA) straddling the first rise of atmospheric oxygen between 2.4 and 2.0 Ga. *Geochimica et Cosmochimica Acta*, **71**, A296–A296.

Frei, R., Dahl, P.S., Duke, E.F., Frei, K.M., Hansen, T.R., Frandsson, M.M. & Jensen, L.A. 2008. Trace element and isotopic characterization of Neoarchean and Paleoproterozoic iron formations in the Black Hills (South Dakota, USA): Assessment of chemical change during 2.9–1.9 Ga deposition bracketing the 2.4–2.2 Ga first rise of atmospheric oxygen. *Precambrian Research*, **162**, 441–474.

Frimmel, H.E. 2008. An evaporitic facies in Neoproterozoic post-glacial carbonates: The Gifberg Group, South Africa. *Gondwana Research*, **13**, 453–468.

German, C.R., Holliday, B.P. & Elderfield, H. 1991. Redox cycling of rare-earth elements in the suboxic zone of the Black Sea. *Geochimica et Cosmochimica Acta*, **55**, 3553–3558.

German, C.R., Higgs, N.C., *et al.* 1993. A geochemical study of metalliferous sediment from the TAG Hydrothermal Mound, 26°08'N, Mid-Atlantic Ridge. *Journal of Geophysical Research, B: Solid Earth*, **98**, 9683–9692.

Giddings, J.A. & Wallace, M.W. 2009. Facies-dependent $\delta^{13}C$ variation from a Cryogenian platform margin, South Australia: Evidence for stratified Neoproterozoic oceans? *Palaeogeography, Palaeoclimatology, Palaeoecology*, **271**, 196–214.

Goddéris, Y., Donnadieu, Y., *et al.* 2003. The Sturtian 'snowball' glaciation: fire and ice. *Earth and Planetary Science Letters*, **211**, 1–12.

Halverson, G.P., Maloof, A.C. & Hoffman, P.F. 2004. The Marinoan glaciation (Neoproterozoic) in northeast Svalbard. *Basin Research*, **16**, 297–324.

Hild, E. & Brumsack, H.-J. 1998. Major and minor element geochemistry of Lower Aptian sediments from the NW German Basin (core Hohenegglesen KB 40). *Cretaceous Research*, **19**, 615–633.

Hoffman, P.F. & Schrag, D.P. 2002. The snowball Earth hypothesis: testing the limits of global change. *Terra Nova*, **14**, 129–155.

Hoffman, P.F., Halverson, G.P., Domack, E.W., Husson, J.M., Higgins, J.A. & Schrag, D.P. 2007. Are basal Ediacaran (635 Ma) post-glacial 'cap dolostones' diachronous? *Earth and Planetary Science Letters*, **258**, 114–131.

Hoffmann, K.-H., Condon, D.J., Bowring, S.A. & Crowley, J.L. 2004. U–Pb zircon date from the Neoproterozoic Ghaub Formation, Namibia: Constraints on Marinoan glaciation. *Geology*, **32**, 817–820.

Huang, J., Chu, X.L., Chang, H.J. & Feng, L.J. 2009. Trace element and rare earth element of cap carbonate in Ediacaran Doushantuo Formation in Yangtze Gorges. *Chinese Science Bulletin*, **54**, 3295–3302.

Hurtgen, M.T., Halverson, G.P., Arthur, M.A. & Hoffman, P.F. 2006. Sulfur cycling in the aftermath of a 635-Ma snowball glaciation: Evidence for a syn-glacial sulfidic deep ocean. *Earth and Planetary Science Letters*, **245**, 551–570.

Ilyin, A.V. 2009. Neoproterozoic banded iron formations. *Lithology and Mineral Resources*, **44**, 78–86.

Jacobsen, S.B. & Kaufman, A.J. 1999. The Sr, C and O isotopic evolution of Neoproterozoic seawater. *Chemical Geology*, **161**, 37–57.

James, N.P., Narbonne, G.M. & Kyser, T.K. 2001. Late Neoproterozoic cap carbonates: Mackenzie Mountains, northwestern Canada: precipitation and global glacial meltdown. *Canadian Journal of Earth Sciences*, **38**, 1229–1262.

Jiang, G.Q., Kennedy, M.J. & Christie-Blick, N. 2003*a*. Stable isotopic evidence for methane seeps in Neoproterozoic postglacial cap carbonates. *Nature*, **426**, 822–826.

Jiang, G.Q., Sohl, L.E. & Christie-Blick, N. 2003*b*. Neoproterozoic stratigraphic comparison of the Lesser Himalaya (India) and Yangtze block (south China):

Paleogeographic implications. *Geology*, **31**, 917–920.

Jiang, G.Q., Kennedy, M.J., Christie-Blick, N., Wu, H.C. & Zhang, S.H. 2006*a*. Stratigraphy, sedimentary structures and textures of the late Neoproterozoic Doushantuo cap carbonate in south China. *Journal of Sedimentary Research*, **76**, 978–995.

Jiang, G.Q., Shi, X.Y. & Zhang, S.H. 2006*b*. Methane seeps, methane hydrate destabilization and the late Neoproterozoic postglacial cap carbonates. *Chinese Science Bulletin*, **51**, 1152–1173.

Johnston, D.T., Poulton, S.W., Dehler, C., Porter, S., Husson, J., Canfield, D.E. & Knoll, A.H. 2010. An emerging picture of Neoproterozoic ocean chemistry: Insights from the Chuar Group, Grand Canyon, USA. *Earth and Planetary Science Letters*, **290**, 64–73.

Kamber, B.S. & Webb, G.E. 2001. The geochemistry of late Archaean microbial carbonate: Implications for ocean chemistry and continental erosion history. *Geochimica et Cosmochimica Acta*, **65**, 2509–2525.

Kaufman, A.J. & Knoll, A.H. 1995. Neoproterozoic variations in the C-isotopic composition of seawater: stratigraphic and biogeochemical implications. *Precambrian Research*, **73**, 27–49.

Kaufman, A.J., Knoll, A.H. & Narbonne, G.M. 1997. Isotopes, ice ages and terminal Proterozoic Earth history. *Proceedings of the National Academy of Sciences of the USA*, **94**, 6600–6605.

Kennedy, M.J. 1996. Stratigraphy, sedimentology and isotopic geochemistry of Australian Neoproterozoic postglacial cap dolostones; Deglaciation, $\delta^{13}C$ excursions and carbonate precipitation. *Journal of Sedimentary Research*, **66**, 1050–1064.

Kennedy, M.J., Christie-Blick, N. & Sohl, L.E. 2001. Are Proterozoic cap carbonates and isotopic excursions a record of gas hydrate destabilization following Earth's coldest intervals? *Geology*, **29**, 443–446.

Kirschvink, J.L. 1992. Late Proterozoic low-latitude global glaciation: the snowball earth. *In:* Schopf, J.W. & Klein, C. (eds) *The Proterozoic Biosphere: A Multidisciplinary Study*. Cambridge University Press, Cambridge, 51–52.

Klein, C. 2005. Some Precambrian banded iron-formations (BIFs) from around the world: Their age, geologic setting, mineralogy, metamorphism, geochemistry and origin. *American Mineralogist*, **90**, 1473–1499.

Klein, C. & Ladeira, E.A. 2004. Geochemistry and mineralogy of Neoproterozoic banded iron-formations and some selected, siliceous manganese formations from the Urucum district, Mato Grosso do Sul, Brazil. *Economic Geology*, **99**, 1233–1244.

Kump, L.R. & Seyfried, W.E. Jr 2005. Hydrothermal Fe fluxes during the Precambrian: Effect of low oceanic sulfate concentrations and low hydrostatic pressure on the composition of black smokers. *Earth and Planetary Science Letters*, **235**, 654–662.

Lawrence, M.G., Greig, A., Collerson, K.D. & Kamber, B.S. 2006. Rare earth element and yttrium variability in south east Queensland waterways. *Aquatic Geochemistry*, **12**, 39–72.

Li, C., Love, G.D., Lyons, T.W., Fike, D.A., Sessions, A.L. & Chu, X.L. 2010. A stratified redox model for the Ediacaran ocean. *Science*, **328**, 80–83.

Lyons, T.W. & Severmann, S. 2006. A critical look at iron paleoredox proxies: New insights from modern euxinic marine basins. *Geochimica et Cosmochimica Acta*, **70**, 5698–5722.

McLennan, S.M. 1989. Rare earth elements in sedimentary rocks: influence of provenance and sedimentary processes. *In:* Lipin, B.R. & McKay, G.A. (eds) *Geochemistry and Mineralogy of Rare Earth Elements*. Mineralogical Society of America, Reviews in Mineralogy, **21**, 169–200.

Morford, J.L. & Emerson, S. 1999. The geochemistry of redox sensitive trace metals in sediments. *Geochimica et Cosmochimica Acta*, **63**, 1735–1750.

Morford, J.L., Russell, A.D. & Emerson, S. 2001. Trace metal evidence for changes in the redox environment associated with the transition from terrigenous clay to diatomaceous sediment, Saanich Inlet, BC. *Marine Geology*, **174**, 355–369.

Nédélec, A., Affaton, P., France-Lanord, C., Charrière, A. & Alvaro, J. 2007. Sedimentology and chemostratigraphy of the Bwipe Neoproterozoic cap dolostones (Ghana, Volta Basin): A record of microbial activity in a peritidal environment. *Comptes Rendus Géoscience*, **339**, 223–239.

Nogueira, A.C.R., Riccomini, C., Sial, A.N., Moura, C.A.V. & Fairchild, T.R. 2003. Soft-sediment deformation at the base of the Neoproterozoic Puga cap carbonate (southwestern Amazon craton, Brazil): Confirmation of rapid icehouse to greenhouse transition in snowball Earth. *Geology*, **31**, 613–616.

Nothdurft, L.D., Webb, G.E. & Kamber, B.S. 2004. Rare earth element geochemistry of Late Devonian reefal carbonates, Canning Basin, Western Australia: confirmation of a seawater REE proxy in ancient limestones. *Geochimica et Cosmochimica Acta*, **68**, 263–283.

Roy, S. 2006. Sedimentary manganese metallogenesis in response to the evolution of the Earth system. *Earth-Science Reviews*, **77**, 273–305.

Shen, B., Xiao, S.H., Kaufman, A.J., Bao, H.M., Zhou, C.M. & Wang, H.F. 2008. Stratification and mixing of a post-glacial Neoproterozoic ocean: Evidence from carbon and sulfur isotopes in a cap dolostone from northwest China. *Earth and Planetary Science Letters*, **265**, 209–228.

Shen, Y., Zhang, T.G. & Chu, X.L. 2005. C-isotopic stratification in a Neoproterozoic postglacial ocean. *Precambrian Research*, **137**, 243–251.

Shields, G.A. 2005. Neoproterozoic cap carbonates: a critical appraisal of existing models and the plumeworld hypothesis. *Terra Nova*, **17**, 299–310.

Sholkovitz, E.R., Piepgras, D.J. & Jacobsen, S.B. 1989. The pore water chemistry of rare earth elements in Buzzards Bay sediments. *Geochimica et Cosmochimica Acta*, **53**, 2847–2856.

Slack, J.F., Grenne, T., Bekker, A., Rouxel, O.J. & Lindberg, P.A. 2007. Suboxic deep seawater in the late Paleoproterozoic: Evidence from hematitic chert and iron formation related to seafloor–hydrothermal sulfide deposits, central Arizona, USA. *Earth and Planetary Science Letters*, **255**, 243–256.

Tanaka, K. & Kawabe, I. 2006. REE abundances in ancient seawater inferred from marine limestone and experimental REE partition coefficients between calcite and aqueous solution. *Geochemical Journal*, **40**, 425–435.

Tribovillard, N., Desprairies, A., Lallier-Vergès, E., Bertrand, P., Moureau, N., Ramdani, A. & Ramanampisoa, L. 1994. Geochemical study of organic-matter rich cycles from the Kimmeridge Clay Formation of Yorkshire (UK)—productivity versus anoxia. *Palaeogeography, Palaeoclimatology, Palaeoecology*, **108**, 165–181.

Tribovillard, N., Algeo, T.J., Lyons, T.W. & Riboulleau, A. 2006. Trace metals as paleoredox and paleoproductivity proxies: An update. *Chemical Geology*, **232**, 12–32.

Von Damm, K.L. 1995. Controls on the chemistry and temporal variability of seafloor hydrothermal fluids. *In:* Humphris, S.E., Zierenberg, R.A., Mullineaux, L.S. & Thomson, R.E. (eds) *Seafloor Hydrothermal Systems: Physical, Chemical, Biological and Geological Interactions*. American Geophysical Union, Geophysical Monograph, **91**, 222–247.

Wang, J. & Li, Z.X. 2003. History of Neoproterozoic rift basins in South China: implications for Rodinia break-up. *Precambrian Research*, **122**, 141–158.

Wang, J.S., Jiang, G.Q., Xiao, S.H., Li, Q. & Wei, Q. 2008. Carbon isotope evidence for widespread methane seeps in the *ca*. 635 Ma Doushantuo cap carbonate in south China. *Geology*, **36**, 347–350.

Webb, G.E. & Kamber, B.S. 2000. Rare earth elements in Holocene reefal microbialites: a new shallow seawater proxy. *Geochimica et Cosmochimica Acta*, **64**, 1557–1565.

Webb, G.E., Nothdurft, L.D., Kamber, B.S., Kloprogge, J.T. & Zhao, J.X. 2009. Rare earth element geochemistry of scleractinian coral skeleton during meteoric diagenesis: a sequence through neomorphism of aragonite to calcite. *Sedimentology*, **56**, 1433–1463.

Xiao, S.H., Bao, H.M., *et al.* 2004. The Neoproterozoic Quruqtagh Group in eastern Chinese Tianshan: evidence for a post-Marinoan glaciation. *Precambrian Research*, **130**, 1–26.

Yin, C.Y., Tang, F., *et al.* 2005. U–Pb zircon age from the base of the Ediacaran Doushantuo Formation in the Yangtze Gorges, South China: constraint on the age of Marinoan glaciation. *Episodes*, **28**, 48–49.

Yoshioka, H., Asahara, Y., Tojo, B. & Kawakami, S. 2003. Systematic variations in C, O and Sr isotopes and elemental concentrations in Neoproterozoic carbonates in Namibia: implications for a glacial to interglacial transition. *Precambrian Research*, **124**, 69–85.

Zhang, S.H., Jiang, G.Q., Zhang, J.M., Song, B., Kennedy, M.J. & Christie-Blick, N. 2005. U–Pb sensitive high-resolution ion microprobe ages from the Doushantuo Formation in south China: Constraints on late Neoproterozoic glaciations. *Geology*, **33**, 473–476.

Zhao, Y.Y., Zheng, Y.F. & Chen, F.K. 2009. Trace element and strontium isotope constraints on sedimentary environment of Ediacaran carbonates in southern Anhui, South China. *Chemical Geology*, **265**, 345–362.

Zhong, S.J. & Mucci, A. 1995. Partitioning of rare-earth elements (REEs) between calcite and seawater solutions at 25 °C and 1 atm, and high dissolved REE concentrations. *Geochimica et Cosmochimica Acta*, **59**, 443–453.

Zhou, C.M. & Xiao, S.H. 2007. Ediacaran delta $\delta^{13}C$ chemostratigraphy of South China. *Chemical Geology*, **237**, 89–108.

Received 10 August 2010; revised typescript accepted 30 November 2010.
Scientific editing by James Hendry.